Collision-Induced Spin Exchange of Alkali-Metal Atoms With \(^3\)He: An Ab Initio Study

Collision-induced spin exchange of alkali-metal atoms with ^{3}He: An *ab initio* study

T. V. Tscherbul,[1,2,*] P. Zhang,[2] H. R. Sadeghpour,[2] and A. Dalgarno[1,2]
[1]*Harvard-MIT Center for Ultracold Atoms, Cambridge, Massachusetts 02138, USA*
[2]*Institute for Theoretical Atomic, Molecular, and Optical Physics, Harvard-Smithsonian Center for Astrophysics, Cambridge, Massachusetts 02138, USA*
(Received 5 March 2009; published 9 June 2009)

We present a rigorous quantum study of spin-exchange transitions in collisions of the alkali-metal atoms with ^{3}He in the presence of an external magnetic field. Using accurate *ab initio* interaction potentials, we obtain refined estimates for the Fermi contact interaction constants for complexes of Na, K, and Rb atoms with ^{3}He. *Ab initio* calculations show that the Fermi contact interaction in Li-^{3}He varies more slowly with internuclear distance than predicted by the atomic model [R. M. Herman, Phys. Rev. **37**, A1062 (1965)]. The calculated spin-exchange rate constants for Na, K, and Rb atoms in a gas of ^{3}He are in good agreement with experimental data. Our calculations demonstrate that at a temperature of 0.5 K, collision-induced spin exchange of the alkali-metal atoms occurs at a very slow rate of $\sim 10^{-22}$ cm^3/s, suggesting potential applications in cryogenic cooling, precision spectroscopy, and quantum optics.

DOI: 10.1103/PhysRevA.79.062707 PACS number(s): 34.50.−s

I. INTRODUCTION

Collisions of atoms and molecules in the presence of external electromagnetic fields may lead to depolarization of their electronic and nuclear spins, causing decoherence of quantum superposition states [1,2], reduction in the lifetime of trapped atoms [3,4], and frequency shifts in atomic clocks and magnetometers [1]. The fundamental microscopic processes that give rise to spin depolarization are spin exchange and spin relaxation [5]. While the former process merely transfers spin polarization from one atom to another [1,5], the latter results in loss of polarization via the interaction of the electron spin with the orbital angular momentum of the collision complex [6]. Due to their importance to spectroscopic measurements based on alkali-metal vapor cells, both mechanisms have attracted much experimental and theoretical attention [1–6].

The experimental technique of spin-exchange optical pumping (SEOP) makes use of spin-exchange collisions to produce hyperpolarized ^{3}He nuclei for studies in neutron physics [7], surface science [5], and medical imaging [8]. The efficiency of SEOP is determined by the ratio of the rate constants for spin exchange and spin relaxation in alkali-metal–^{3}He collisions. The spin-exchange and spin-relaxation rates for different alkali-metal atoms were measured in several experiments [9–14]. Ben-Amar Baranga *et al.* [9] studied collisions of optically pumped Rb atoms with ^{3}He in a cell and measured the rate constant for spin exchange in Rb-^{3}He collisions to be 6.1×10^{-20} cm^3/s. More recent experiments found no observable temperature dependence of the rate constant [10,11]. Recent room-temperature measurements of spin-depolarization rates for K [12,13] and Na [14] in ^{3}He buffer gas yielded spin-exchange rates of 6×10^{-20} cm^3/s, very similar to those obtained for Rb.

The decoherence of atomic states brought about by spin depolarization is important in quantum optics, precision spectroscopy, and quantum information processing. Recently, Hong *et al.* [2] demonstrated a new coherent optical medium based on Rb vapor mixed with cold ^{4}He gas at 4 K. Collision-induced spin depolarization may induce decoherence of quantum superposition states in such a system. Sushkov and Budker [15] used laser ablation to produce cold samples of Li and Rb atoms inside a buffer-gas cell and observed an unexplained atom loss mechanism. In cryogenic cooling and magnetic trapping experiments, spin-changing collisions lead to loss of atoms and molecules from the trap [3,4,16]. It is therefore essential to find ways to minimize the negative impact of collisional spin depolarization in these experiments.

Early theoretical studies have shown that spin exchange in binary collisions occurs due to the Fermi contact hyperfine interaction of the alkali-metal valence electron with the nuclear spin of ^{3}He [17,18]. The strength of the Fermi contact interaction is proportional to the electron-spin density of the atom-He complex at the He nucleus [17]. Herman [17] demonstrated that the electron-spin density in alkali-metal–He complexes is enhanced with respect to that in free alkali-metal atoms by a factor $\eta > 1$. The enhancement occurs because of the exchange interaction of the valence electron with the ^{3}He core. Based on the assumption that η does not depend on the alkali-metal atom (M) and the internuclear distance in the M-He complex, Herman [17] obtained $|\eta| \approx 7$. In 1989, Walker [19] improved this estimate using approximate M-He interaction potentials and semiclassical models for collision dynamics. His result was $|\eta| = 9.5$. More recently, the estimate was further refined using highly accurate polarimetry experiments [20,21]. However, all of these estimates suffered from the uncertainties in the M-He interaction potentials used to reconstruct η from the measured spin-exchange cross sections and frequency shift enhancement factors.

We have recently reported an *ab initio* study of spin exchange in M-He collisions using accurate interaction potentials and improved estimates of the Fermi contact interaction parameters [22]. We have found that the model of Herman

*tshcherb@cfa.harvard.edu

[17] provides an adequate description of the electron-spin density for the Li-He system with $\eta=2.5$. In order to infer η for the heavier alkali-metal atoms, we used recent experimental measurements of frequency shift enhancement factors to extract refined values of $\eta=2.0$ for Na-He and $\eta=1.85$ for K-He. Our calculated spin-exchange cross sections are consistent with the upper bounds derived from magnetic trapping experiments with spin-polarized ^{39}K and ^{7}Li atoms at subkelvin temperatures [22]. At higher temperatures, the theoretical spin-exchange rate constants for K-He are in good agreement with the values measured in spin-exchange optical pumping experiments.

This work is an extension of our previous Rapid Communication [22]. We present a rigorous analysis of spin-exchange transitions in collisions of the alkali-metal atoms (Li to Rb) with ^{3}He. We use accurate *ab initio* calculations to evaluate the electron-spin density of Li-He and the interaction energy of Rb-He. The Fermi contact interaction constants (FCICs) for the complexes of Na, K, and Rb atoms with ^{3}He are extracted from the measured frequency shift enhancement factors using the *ab initio* interaction potentials. The spin-density calculations also yield the hyperfine pressure shift of Li-He, which allows us to test a perturbative model for this quantity, recently proposed by Oreto *et al.* [23]. We find that the calculated temperature dependence of the spin-exchange rates for Na, K, and Rb atoms in a buffer gas of He is steeper than that measured experimentally. We demonstrate that this behavior can be attributed to a subtle drawback of the atomic model [17].

In Sec. II we describe the quantum-mechanical theory of spin exchange in atom-atom collisions. The theory is applied to calculate the cross sections and rate constants for spin exchange in collisions of the alkali-metal atoms with He in Sec. III. The paper concludes with a brief summary of the main findings (Sec. IV). Atomic units are used throughout unless indicated otherwise.

II. THEORY

Collision dynamics

The Hamiltonian of the atom-He collision complex in the presence of an external magnetic field can be written as [5,24]

$$\hat{H} = -\frac{1}{2\mu R}\frac{\partial^2}{\partial R^2}R + \frac{\hat{\ell}^2}{2\mu R^2} + V(R) + \hat{H}_{\rm sd} + \hat{H}_M + \hat{H}_{\rm He}, \quad (1)$$

where M denotes the alkali-metal atom, μ is the reduced mass of the M-He complex, R is the interatomic distance, $\hat{\ell}$ is the orbital angular momentum for the collision, and $V(R)$ is the electrostatic (spin-independent) interaction potential. The Hamiltonian of the isolated alkali-metal atom can be written as

$$\hat{H}_M = A\hat{I}\cdot\hat{S} + 2\mu_0 B\hat{S}_z - B\frac{\mu_M}{I}\hat{I}_z, \quad (2)$$

where A is the hyperfine constant, μ_0 is the Bohr magneton, μ_M is the nuclear magnetic moment of M, and the operators $\hat{S}_z$ and $\hat{I}_z$ yield z components of the electron and nuclear spins. We choose the space-fixed quantization axis z along the direction of the external magnetic field B. The interaction of the nuclear spin of ^{3}He ($\hat{I}_{\rm He}$) with the magnetic field is described by the Hamiltonian

$$\hat{H}_{\rm He} = -B\frac{\mu_{\rm He}}{I_{\rm He}}\hat{I}_{{\rm He}_z}. \quad (3)$$

The spin-dependent part of Hamiltonian (1) is given by [5,24]

$$\hat{H}_{\rm sd} = A_{\rm F}(R)\hat{I}_{\rm He}\cdot\hat{S} + \gamma(R)\hat{\ell}\cdot\hat{S} + \Delta A(R)\hat{I}\cdot\hat{S}, \quad (4)$$

where the first term on the right-hand side describes the Fermi contact hyperfine interaction between the electron spin of M and the nuclear spin of ^{3}He ($I_{\rm He}=1/2$). The second term is the spin-rotation interaction, which couples the orbital angular momentum of the collision complex and the electron spin of M. This interaction causes the electron-spin polarization to decay with time, but does not affect the nuclear-spin polarization of He. For this reason, the rate constants for spin exchange and spin relaxation can be measured separately in SEOP experiments [9–14]. A theoretical analysis of the spin-relaxation mechanism is beyond the scope of this work. The last term in Eq. (4) describes the modification of the hyperfine constant of M due to the approach of the He atom. Accurate *ab initio* calculations of the Fermi contact interaction constant and the hyperfine pressure shift for Li-He are presented in Sec. III.

The total wave function for the collision is expanded as

$$\Psi = \frac{1}{R}\sum_{\beta}\sum_{\ell,m_\ell} F_{\beta\ell m_\ell}(R)|\beta\rangle|\ell m_\ell\rangle, \quad (5)$$

where the partial waves $|\ell m_\ell\rangle$ describe the orbital motion of the collision partners and

$$|\beta\rangle = |IM_I\rangle|SM_S\rangle|I_{\rm He}M_{I_{\rm He}}\rangle \quad (6)$$

are the fully uncoupled space-fixed basis functions. In this expression, $|SM_S\rangle$ and $|IM_I\rangle$ are the electron- and nuclear-spin basis functions of atom M and $|I_{\rm He}M_{I_{\rm He}}\rangle$ are the nuclear-spin basis functions for He. The total angular momentum projection $M_{\rm tot}=M_I+M_S+M_{I_{\rm He}}+m_\ell$ is conserved. Substituting the above expansion into the time-independent Schrödinger equation with Hamiltonian (1), we obtain the system of close-coupling (CC) equations

$$\left[\frac{d^2}{dR^2} - \frac{\ell(\ell+1)}{R^2} + 2\mu E\right]F_{\beta\ell m_\ell}(R) = 2\mu\sum_{\beta'}\sum_{\ell',m'_\ell}\langle\beta\ell m_\ell|V(R) + \hat{H}_{\rm sd}(R) + \frac{\hat{\ell}^2}{2\mu R^2} + \hat{H}_M + \hat{H}_{\rm He}|\beta'\ell' m'_\ell\rangle F_{\beta'\ell' m'_\ell}(R), \quad (7)$$

where E is the total energy. We describe below the evaluation of the matrix elements on the right-hand side of Eq. (7). The interaction potential and the centrifugal kinetic energy are both diagonal in uncoupled basis (5), with the matrix ele-

ments $\delta_{\beta\beta'}\delta_{\ell\ell'}\delta_{m_\ell m'_\ell}V(R)$ and $\delta_{\beta\beta'}\delta_{\ell\ell'}\delta_{m_\ell m'_\ell}\ell(\ell+1)/2\mu R^2$. The off-diagonal matrix elements of alkali-metal Hamiltonian (2) are due to the hyperfine interaction, which couples different M_I and M_S,

$$\begin{aligned}\langle\beta|\hat{H}_M|\beta'\rangle = {} & \delta_{M_I M'_I}\delta_{M_S M'_S}\delta_{M_{I_{\mathrm{He}}},M'_{I_{\mathrm{He}}}} \\ & \times\left[AM_IM_S + 2\mu_0 BM_S - B\frac{\mu_M}{I}M_I\right] \\ & + \frac{1}{2}A\delta_{M_{I_{\mathrm{He}}},M'_{I_{\mathrm{He}}}}[I(I+1) - M'_I(M'_I \pm 1)]^{1/2} \\ & \times[S(S+1) - M'_S(M'_S \mp 1)]^{1/2}\delta_{M_I,M'_I\pm 1}\delta_{M_S,M'_S\mp 1}.\end{aligned} \tag{8}$$

The interaction of the nuclear spin of ^{3}He with magnetic field has the following matrix elements:

$$\langle\beta|\hat{H}_{\mathrm{He}}|\beta'\rangle = -\delta_{M_{I_{\mathrm{He}}},M'_{I_{\mathrm{He}}}}\delta_{M_S M'_S}\delta_{M_I M'_I}B\frac{\mu_{\mathrm{He}}}{I_{\mathrm{He}}}M_{\mathrm{He}}. \tag{9}$$

The Fermi contact hyperfine interaction can be expressed through the raising and lowering operators as

$$A_{\mathrm{F}}(R)\hat{I}_{\mathrm{He}}\cdot\hat{S} = A_{\mathrm{F}}(R)\left[\hat{I}_{\mathrm{He}_z}\hat{S}_z + \tfrac{1}{2}(\hat{I}_{\mathrm{He}_-}\hat{S}_+ + \hat{I}_{\mathrm{He}_+}\hat{S}_-)\right]. \tag{10}$$

This expression shows that the Fermi contact interaction couples the states with different M_S and $M_{I_{\mathrm{He}}}$. Noting that Eq. (10) is diagonal in ℓ and m_ℓ, we obtain an expression analogous to Eq. (8),

$$\begin{aligned}&\langle\beta|A_{\mathrm{F}}(R)\hat{I}_{\mathrm{He}}\cdot\hat{S}|\beta'\rangle \\ &\quad = \Big\{M_{I_{\mathrm{He}}}M_S\delta_{M_S M'_S}\delta_{M_{I_{\mathrm{He}}},M'_{I_{\mathrm{He}}}} + \tfrac{1}{2}[I_{\mathrm{He}}(I_{\mathrm{He}}+1) \\ &\qquad - M'_{I_{\mathrm{He}}}(M'_{I_{\mathrm{He}}} \pm 1)]^{1/2}[S(S+1) \\ &\qquad - M'_S(M'_S \mp 1)]^{1/2}\delta_{M_{I_{\mathrm{He}}},M'_{I_{\mathrm{He}}}\pm 1}\delta_{M_S,M'_S\mp 1}\Big\}\delta_{M_I M'_I}A_{\mathrm{F}}(R).\end{aligned} \tag{11}$$

The matrix elements of the third term in Eq. (4) can be written as

$$\begin{aligned}&\langle\beta|\Delta A(R)\hat{I}\cdot\hat{S}|\beta'\rangle \\ &\quad = \Big\{M_I M_S\delta_{M_S M'_S}\delta_{M_I M'_I} + \tfrac{1}{2}[I(I+1) \\ &\qquad - M'_I(M'_I \pm 1)]^{1/2}[S(S+1) - M'_S(M'_S \mp 1)]^{1/2} \\ &\qquad \times\delta_{M_I,M'_I\pm 1}\delta_{M_S,M'_S\mp 1}\Big\}\delta_{M_{I_{\mathrm{He}}},M'_{I_{\mathrm{He}}}}\Delta A(R).\end{aligned} \tag{12}$$

In order to verify our results, we performed scattering calculations in a coupled basis

$$|Fm_F\rangle|I_{\mathrm{He}}M_{I_{\mathrm{He}}}\rangle|\ell m_\ell\rangle, \tag{13}$$

where $\hat{F}=\hat{I}+\hat{S}$ is the total angular momentum of atom M and $m_F=M_I+M_S$. The expressions for the matrix elements in the coupled basis are given in the Appendix.

It follows from Eq. (8) that the asymptotic Hamiltonian $\hat{H}_{\mathrm{as}}=\hat{H}_M+\hat{H}_{\mathrm{He}}$ is not diagonal in uncoupled basis (6). In order to apply the scattering boundary conditions, we must transform the wave function from uncoupled representation (6) to the eigenchannel representation

$$|\gamma\rangle|\ell m_\ell\rangle = |\ell m_\ell\rangle\sum_\beta C_{\beta\gamma}|\beta\rangle. \tag{14}$$

The coefficients $C_{\beta\gamma}$ make up an orthogonal matrix, which diagonalizes the asymptotic Hamiltonian at each value of the magnetic field,

$$\langle\gamma\ell m_\ell|\hat{H}_{\mathrm{as}}|\gamma'\ell' m'_\ell\rangle = \delta_{\ell\ell'}\delta_{m_\ell m'_\ell}\delta_{\gamma\gamma'}\epsilon_\gamma, \tag{15}$$

where $\epsilon_\gamma=\epsilon_M+\epsilon_{\mathrm{He}}$ are the Zeeman energies of two noninteracting atoms. Property (15) allows us to apply the standard boundary conditions for inelastic scattering,

$$\begin{aligned}F_{\gamma\ell m_\ell;\gamma'\ell' m'_\ell}(R\to\infty) \to {} & k_\gamma^{-1/2}\{\delta_{\gamma\gamma'}\delta_{\ell\ell'}\delta_{m_\ell m'_\ell} \\ & \times\exp[-i(k_\gamma R - \ell\pi/2)] + S_{\gamma'\ell' m'_\ell;\gamma\ell m_\ell} \\ & \times\exp[i(k_{\gamma'}R - \ell'\pi/2)]\},\end{aligned} \tag{16}$$

where $k_\gamma^2=2\mu(E-\epsilon_\gamma)=2\mu E_{\mathrm{c}}$ is the wave vector, E_{c} is the collision energy, $F_{\gamma\ell m_\ell;\gamma'\ell' m'_\ell}(R)$ are radial expansion coefficients (5) in eigenchannel representation (14), and $S_{\gamma'\ell' m'_\ell;\gamma\ell m_\ell}$ are the S-matrix elements. The integral cross sections for collision-induced transitions between the different Zeeman states of M and ^{3}He can be written as

$$\sigma_{\gamma\to\gamma'}(E_{\mathrm{c}}) = \frac{\pi}{k^2_{\gamma M_{\mathrm{tot}},\ell}}\sum_{m_\ell,m'_\ell}\sum|\delta_{\ell\ell'}\delta_{m_\ell m'_\ell}\delta_{\gamma\gamma'} - S^{M_{\mathrm{tot}}\ell}_{\gamma' m'_\ell;\gamma m_\ell}|^2, \tag{17}$$

where we can write $S_{\gamma\ell m_\ell;\gamma'\ell' m'_\ell}=S^{M_{\mathrm{tot}}\ell}_{\gamma m_\ell;\gamma' m'_\ell}$ since both ℓ and M_{tot} are conserved quantities.

The CC equations (7) were solved numerically using the improved log-derivative method [25]. The wave function was propagated from $R=3a_0$ to $R=50a_0$ with a step size of $0.04a_0$. In order to ensure convergence of spin-exchange cross sections to better than 5%, up to 180 terms were included in partial wave expansion (5), leading to 16 coupled equations for $\ell\geq 3$ and $|M_{\mathrm{tot}}|=\frac{1}{2}$. To ensure convergence of the cross sections at collision energies below 1 K, it was necessary to propagate the CC equations out to $200a_0$. As a further check of our results, we compared the calculated elastic cross sections with the experimental data for Li-He [26] and found good agreement.

III. RESULTS

In this section, we apply the theory outlined above to collisions of the alkali-metal atoms with He. We parametrize the scattering Hamiltonian using realistic atom-atom interaction potentials, Fermi contact interaction constants, and hyperfine pressure shifts for the alkali-metal atoms interacting with He. For Rb-He, we present *ab initio* calculations of the interaction potential. For Li-He, we evaluate both the Fermi contact interaction constant and the hyperfine pressure shift and compare our results with the previous theoretical estimates.

A. Interaction potentials

The potential-energy curves for the interaction of Li, Na, and K atoms with He were calculated by Partridge *et al.* [27] using highly accurate *ab initio* methods. For scattering calculations, we fitted the *ab initio* data points [27] to the analytical form

$$V(R) = e^{-\alpha R+\beta}\sum_{n=0}^{8} a_n R^n - \frac{1}{2}[1+\tanh(\gamma R)]\sum_{n=3}^{6}\frac{C_{2n}}{R^{2n}}. \quad (18)$$

The fitting parameters α, β, a_n, and C_n were optimized using the Levenberg-Marquardt algorithm [28]. The proper asymptotic behavior of $V(R)$ is ensured by using the accurate C_6 dispersion coefficients for the alkali-metal atoms with He calculated by Zhu *et al.* [29]. During the fitting procedure, the parameter C_6 was kept fixed and all other parameters were allowed to vary. For Li-He, we found that setting $C_6=24.47$ produces the best quality fit. This value is slightly larger than that recommended in Ref. [29] ($C_6=22.51$). The deviation of our fits from *ab initio* data [27] does not exceed 0.1% in the region of potential minimum. The fitting parameters are available from the authors upon request.

In order to obtain accurate interaction energies for Rb-He, we use the coupled-cluster method with single, double, and noniterative triple excitations based on the restricted open-shell Hartree-Fock reference wave function [ROHF-RCCSD(T)] [30,31] with an all-electron approximate relativistic Hamiltonian. We employed the spin-averaged third-order Douglas-Kroll-Hess Hamiltonian [32,33], which yields the best approximation to the total energy for many-electron systems [33]. In our coupled-cluster calculations, the $3d4s4p5s$ electrons of the Rb atom and the $1s$ electrons of the He atom were correlated. A fully uncontracted $(24s20p12d5f4g3h)$ basis set was constructed from $(23s19p11d4f)$ primitives of Roos *et al.* [34] by adding $3g$ polarization functions with exponents of 1.249 336, 0.602 788, and 0.202 028 and $2h$ polarization functions with exponents of 1.436 524 and 0.720 408. The polarization functions were variationally optimized to obtain the ground-state energy of the Rb(^2S) atom. In order to properly describe the long-range interactions, a set of $(spdfgh)$ diffuse functions was added in the even-tempered manner with a factor of 2.5. For the He atom, a fully uncontracted augmented correlation-consistent polarized valence sextuple zeta (aug-cc-pV6Z) basis [35] augmented with a set of $(spdfgh)$ diffuse functions was implemented. (The diffuse functions were defined in the same way as for Rb.) The basis-set superposition error was taken into account using the standard counterpoise correction procedure [36]. By analyzing the asymptotic part of the *ab initio* potential, we obtain $C_6=46.48$, in close agreement with the accurate value of 43.4 [29]. All the coupled-cluster calculations were performed using the MOLPRO 2006.1 suite of quantum chemistry programs [37]. A total of 149 *ab initio* data points were generated in the interval $4.6a_0<R<30a_0$. A cubic spline fit to the *ab initio* points in the inner region was smoothly merged with the asymptotic form $-C_6/R^6$ at $R\geq 30a_0$ to provide a global representation of the interaction potential suitable for scattering calculations.

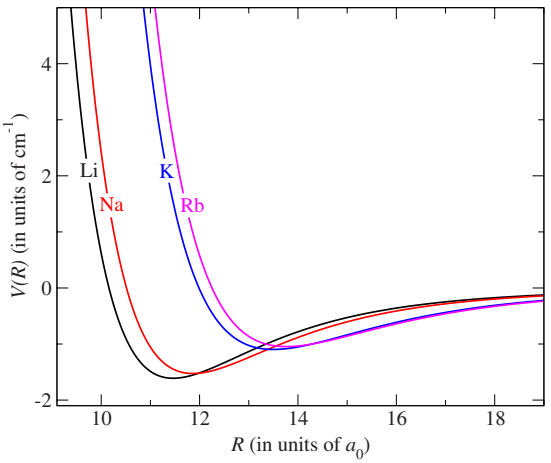

FIG. 1. (Color online) Interaction potentials for the alkali-metal atoms with He. The curves for Li, Na, and K are fits to the *ab initio* data of Ref. [27]. The curve marked "Rb" is a cubic spline approximation to the *ab initio* data points computed in the present work (see text).

Figure 1 shows the *ab initio* potentials for the alkali-metal atoms interacting with He. All the potentials have a van der Waals minimum, which shifts to longer R with increasing mass of the alkali-metal atom. The Li-He system has the largest interaction energy ($D_e=1.6$ cm^{-1}), whereas the Rb-He interaction is the weakest ($D_e=1.0$ cm^{-1}). The inner turning points of the interaction potentials follow the same trend, increasing from $10.2a_0$ (Li-He) to $12.2a_0$ (Rb-He). A comparison of binding energies shows that the interactions of the alkali-metal atoms with He are the most repulsive of all binary atom-He interactions including He-He, for which $D_e=7.65$ cm^{-1} [38]. As a consequence, none of the M-^{3}He interaction potentials supports bound or quasibound states.

B. Fermi contact interaction constants

The Fermi contact interaction constant in Eq. (4) can be written as

$$A_F(R) = \frac{16\pi}{3}\frac{\mu_0\mu_{He}}{I_{He}}\rho_{He}(R), \quad (19)$$

where $\rho_{He}(R)$ is the electron-spin density at the He nucleus defined as the expectation value of the three-dimensional Dirac δ function,

$$\rho_{He}(R) = \langle\psi(\mathbf{r}_e,\sigma_e;R)|\delta(\mathbf{r}_e-\mathbf{R})|\psi(\mathbf{r}_e,\sigma_e;R)\rangle, \quad (20)$$

where $\psi(\mathbf{r}_e,\sigma_e;R)$ is the adiabatic wave function for the ground $^2\Sigma$ electronic state of Li-He, which depends on the spatial ($\mathbf{r}_e$) and spin (σ_e) coordinates of the electrons. The averaging in Eq. (20) is performed over $\mathbf{r}_e$ and σ_e at a fixed nuclear geometry specified by the vector $\mathbf{R}$. The origin of the coordinate system is at the Li nucleus.

The accuracy of the calculated FCICs depends on the choice of the atomic basis and of the procedure used to account for the electron correlation. Two main problems are associated with choosing the optimal basis set. First, the Gaussian basis functions used in molecular electronic struc-

ture calculations may exhibit incorrect behavior near the nucleus (such as the absence of a cusp at the origin), which may lead to underestimation of the electron-spin density at the nucleus. This deficiency can be alleviated by including very tight primitive *s* functions [39]. The second problem concerns the contraction coefficients of the primitive basis functions, which are usually optimized for the computation of energy differences. The basis sets commonly used in *ab initio* calculations are most flexible in the outer valence region. However, the electron-spin density at the nucleus is highly sensitive to the behavior of the basis functions in *both* the valence and core regions. Because tight *s* functions are localized in the core region, the basis sets optimized to calculate FCICs need to be more flexible than those used to calculate energy differences. A well-balanced treatment of the electron correlation is also essential. The FCICs calculated at the Hartree-Fock or many-body perturbation theory (MBPT) level can deviate from the accurate values by as much as 100% [40–42]. Because of the need to augment the basis with tight *s* functions, even a qualitative description of the FCICs in atoms heavier than helium requires proper treatment of the core correlation effects.

Ab initio calculations of the electron-spin density for Li-He are performed using the Mainz-Austin-Budapest version of the ACES II program [43] at the coupled-cluster level of theory based on an unrestricted Hartree-Fock reference wave function (the UHF-UCCSD(T) method [41]). The spin densities at the nuclei were computed with the δ-function formalism from the UCCSD(T) relaxed density matrix [41]. For the He atom, we used a modified augmented correlation-consistent polarized valence quintuple zeta (aug-cc-pV5Z) basis [44] obtained by fully decontracting the *s* functions and adding a sequence of three very tight *s* functions with the exponents forming a geometric progression. For Li, we employed an extended augmented correlation-consistent polarized core-valence quadruple zeta (aug-cc-pCVQZ) basis set [45] obtained by completely decontracting the *s* functions and adding four very tight *s* functions. In both cases, the tight *s* functions were obtained by multiplying the largest *s* exponent of the parent basis set by a factor of 4. Our calculated spin density at the nucleus of the isolated Li atom ($\rho_{\mathrm{Li}}=0.230$) is only 1% less than the value obtained from highly accurate variational calculations using Hylleraas coordinates [46].

For the alkali-metal atoms heavier than Li, we adopted the atomic model

$$\rho_{\mathrm{He}}(R) = |\eta\phi_n(R)|^2, \tag{21}$$

where $\phi_n(R)$ is the wave function of the *ns* valence electron ($n=3-5$ for Na to Rb) at a distance R from the nucleus. In order to estimate the enhancement parameter η, we calculated the frequency shift enhancement factor

$$\kappa_0(T) = \int_0^\infty \rho_{\mathrm{He}}(R) e^{-V(R)/k_{\mathrm{B}}T} 4\pi R^2 dR, \tag{22}$$

where k_{B} is the Boltzmann constant and T is the temperature. The temperature dependence of κ_0 was measured to high accuracy in polarimetry experiments with Na, K, and Rb atoms in a buffer gas of ^{3}He [20,21]. Using the *ab initio* interaction potentials described in Sec. III A to evaluate Eq. (22), we varied η until the calculated frequency enhancement factors matched the experimentally measured values at a given temperature. This procedure gives the best-fit parameters η for each alkali-metal atom. The results presented in Table I show that the optimal values of η vary from 2.0 (Na) to 1.85 (K) and 1.83 (Rb). These values are smaller than the estimates $|\eta|=5.8-12.6$ reported previously [47]. We believe that the origin of the disagreement is due to different interaction potentials used in Refs. [19,47] to extract η from the measured frequency shifts. Indeed, Eq. (22) suggests that κ_0 is highly sensitive to the location of the repulsive wall of the interaction potential.

TABLE I. Measured frequency shift enhancement factors κ_0 for Na, K, and Rb atoms in a gas of He from Refs. [20,21]. The spin-exchange enhancement factors η for each atom are adjusted to reproduce the measured values at a given temperature. See text for a detailed description of Rb-He calculations.

Atom	Temperature (K)	η (adjusted)	κ_0 (Expt.)	Reference
Na	473.15	2.0	4.72 ± 0.09	[20]
K	473.15	1.850	5.99 ± 0.11	[20]
Rb	430.15	1.83	5.99 ± 0.09	[21]

Figure 2 shows the temperature dependence of the frequency shift enhancement factor for Rb-He calculated at three different values of η. The experimentally measured $\kappa_0(T)$ is less steep than that predicted by Eq. (22). The temperature dependence of κ_0 reflects the R dependence of the Fermi contact interaction constant [47]. Therefore, the dependence on R of the Fermi contact interaction calculated using atomic model (21) is too steep. In accordance with this observation, the *ab initio* spin density for Li-He shown in Fig. 3 decreases more gradually with R than predicted by Eq. (21).

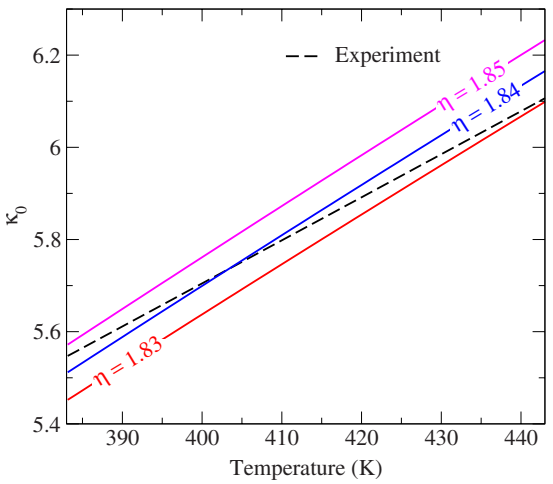

FIG. 2. (Color online) Calculated (solid lines) and measured (dashed line) frequency shift enhancement factors κ_0 [Eq. (22)] as functions of temperature for Rb-He. The values of η are shown in the graph.

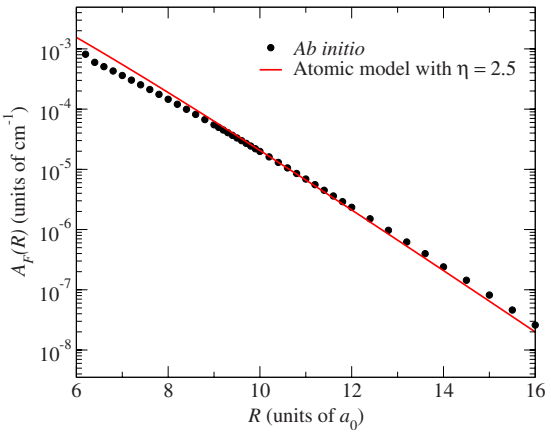

FIG. 3. (Color online) Fermi contact interaction constants as functions of R for Li-^{3}He: *ab initio* calculations (circles) and atomic model (21) parametrized by η=2.5 (full line).

Figure 4 is a plot of the Fermi contact interaction constants for complexes of the alkali-metal atoms with ^{3}He. The hyperfine couplings decrease exponentially with R due to the wave functions on the right-hand side of Eq. (21). The interactions of the Li and Na atoms with the nuclear spin of ^{3}He are significantly weaker than those of K and Rb. This is because the outermost lobes of the electronic wave functions for heavier alkali-metal atoms occur at larger R. However, this difference is compensated for by the fact that the interaction potentials of K and Rb atoms with He are more repulsive (see Fig. 1). As a result, the spin-exchange rates for different alkali-metal atoms are similar as will be shown below.

C. Hyperfine pressure shifts

The hyperfine constant of the alkali-metal atom is modified by the approach of the ^{3}He atom, which gives rise to pressure-dependent frequency shifts of hyperfine levels [5,23]. Such pressure shifts were observed in a number of experiments with alkali-metal vapor cells [5]. Oreto *et al.* [23] recently developed a theoretical approach based on the Fermi contact approximation to estimate the hyperfine pressure shifts. Instead of the quantity $\Delta A(R)$ defined in Eq. (4), it is more convenient to deal with the relative hyperfine pressure shift

$$\delta A_n(R) = \frac{\Delta A_n(R)}{A_n}, \tag{23}$$

where

$$A_n = \frac{16\pi}{3}\frac{\mu_M}{I}\mu_0\rho_{M,n}(R) \tag{24}$$

is the hyperfine constant of the isolated atom in the electronic state characterized by the principal quantum number n and $\rho_{M,n}(R)=|\phi_n(R=0)|^2$ is the spin density at the M nucleus. In the following, $\rho_M(R)$ stands for the electron-spin density for the ground electronic state of Li.

The approach of the ^{3}He atom mixes in other electronic states of higher energy. The contribution from the excited electronic states can be estimated using the Fermi pseudopotential approximation [23]. The final expression for the relative pressure shift can be written in the form

$$\delta A_n(R) = a\sum_{n'>n}\left(\frac{A_{n'}}{A_n}\right)^{1/2}\frac{\phi_n(R)\phi_{n'}(R)}{\epsilon_n-\epsilon_{n'}}, \tag{25}$$

where a is the s-wave scattering length for electron-He collisions, ϵ_n and $\phi_n(R)$ are the energies and wave functions of the atomic states, and A_n are given by Eq. (24). We use the most recent value a=1.17 [48]. Note that only the wave functions of s symmetry need to be included in the summation since the orbitals with $\ell \geq 1$ have zero amplitude at the alkali-metal nucleus. We evaluated Eq. (25) using highly accurate wave functions for Li constructed from a numerical propagation of the Schrödinger equation, in which the interaction of the valence-core electrons was parametrically modeled [49]. A total of 11 terms were included in summation (25), and we verified that reducing the number of terms to 5 does not change the pressure shifts.

In order to test the perturbative expression for the hyperfine pressure shift (25), we performed accurate calculations of the electron-spin density at the Li nucleus using the *ab initio* electronic wave functions for Li-He [cf. Eq. (20)],

$$\rho_M(R) = \langle\psi(\mathbf{r}_e,\sigma_e;R)|\delta(\mathbf{r}_e)|\psi(\mathbf{r}_e,\sigma_e;R)\rangle. \tag{26}$$

Figure 5 compares the *ab initio* hyperfine pressure shifts for Li-He with those given by Eq. (25). The overall agreement is fairly good, although the model of Oreto *et al.* [23] predicts a more gradual increase in the hyperfine shift with decreasing R. The reason for the disagreement can be traced back to the perturbation theory and Fermi contact approximation used to evaluate the contributions from electronically excited states in Eq. (25) [23]. Figure 5 shows that the hyperfine pressure shift given by Eq. (25) is large and negative at small R. The inner turning point of the Li-He interaction potential

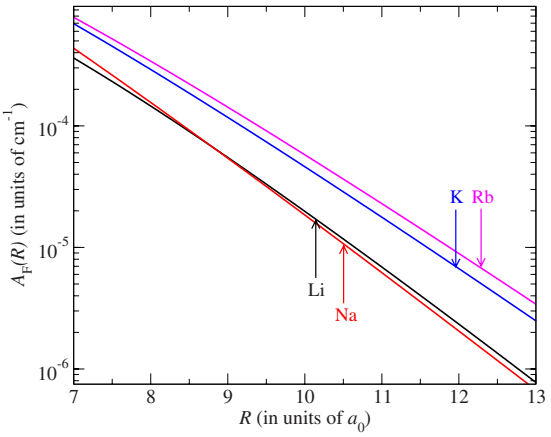

FIG. 4. (Color online) Fermi contact interaction constants as functions of R for complexes of Li, Na, K, and Rb atoms with ^{3}He. The arrows mark the turning points of the M-He interaction potentials (Fig. 1) at zero energy. All the constants (except for Li-He) are calculated using atomic model (21). The corresponding enhancement factors are given in Table I.

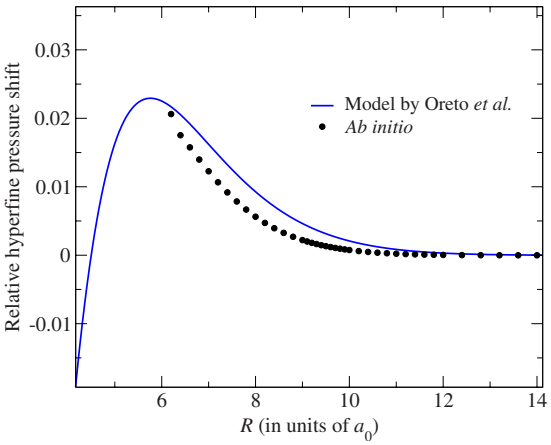

FIG. 5. (Color online) Hyperfine pressure shifts for Li-He calculated *ab initio* (circles) and using the model of Oreto *et al.* [23] (full line).

is located at $R=10.2a_0$ (see Fig. 1), so the region where $\delta A_n(R)$ is negative plays virtually no role in the experiments performed at or below room temperature.

D. Spin-exchange collisions

The spin-exchange transitions occur between the hyperfine levels of the alkali-metal atom and the nuclear-spin levels of the ^{3}He atom. The energy levels of a typical alkali-metal atom with $I=\frac{3}{2}$ (such as the ^{7}Li, ^{23}Na, ^{39}K, and ^{87}Rb atoms studied in this work) are shown in Fig. 6 versus the applied magnetic field. For definiteness, we consider the highest-energy level $|F=2,m_F=2\rangle$ as the initial collision channel. Because the Fermi contact interaction couples the hyperfine states with $\Delta m_F=\pm 1$, spin exchange can occur through the transitions $|F=2,m_F=2\rangle \rightarrow |F'=2,m_F'=1\rangle$ and $|F=2,m_F=2\rangle \rightarrow |F'=1,m_F'=1\rangle$, which are accompanied by

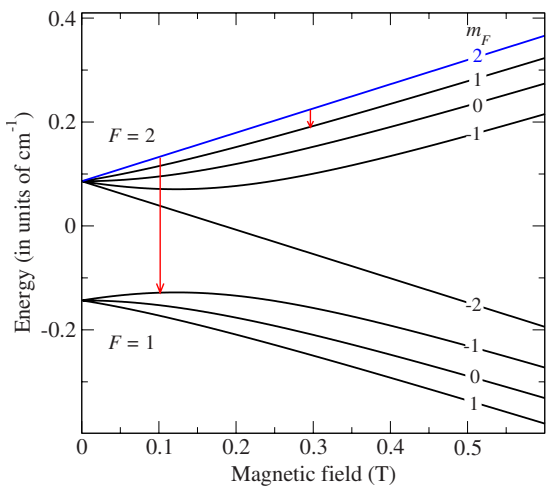

FIG. 6. (Color online) Hyperfine energy levels of ^{87}Rb as functions of the applied magnetic field. The energy-level structure of other alkali-metal atoms studied in this work (^{7}Li, ^{23}Na, and ^{39}K) is similar. The arrows mark the spin-exchange transitions. The initial state for scattering calculations is shown by the uppermost line.

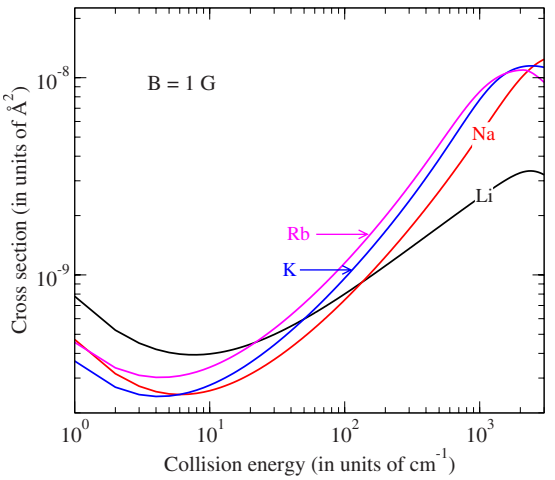

FIG. 7. (Color online) Cross sections for spin exchange in collisions of the alkali-metal atoms with He as functions of collision energy at a magnetic field of 1 G.

the nuclear-spin-changing transition $|M_{I_{\mathrm{He}}}=-\frac{1}{2}\rangle \rightarrow |M'_{I_{\mathrm{He}}}=\frac{1}{2}\rangle$ in ^{3}He. The total spin-exchange cross section is equal to the sum of the cross sections for these two transitions.

The calculated cross sections for spin-exchange transitions in M-He collisions are shown in Fig. 7 as functions of collision energy. The cross sections display broad minima near $E_c=2-10$ cm^{-1} and increase monotonically at $E_c>10$ cm^{-1}. As the collision energy increases, the inner turning point of the M-He interaction potential shifts to smaller R where the Fermi contact interaction is stronger (see Figs. 2 and 3), leading to the enhancement of spin-exchange transitions at high collision energies. The spin-exchange rate constants shown in Fig. 8 increase monotonically with temperature and follow the trend $\Gamma_{\mathrm{Na}}<\Gamma_{\mathrm{K}}<\Gamma_{\mathrm{Rb}}$. Thus, Rb has the largest spin-exchange rate of all alkali-metal atoms over the temperature interval of 1–400 K.

As with the frequency shift enhancement factors (Sec. III B), the temperature dependence of spin-exchange rates is sensitive to the R dependence of the Fermi contact interac-

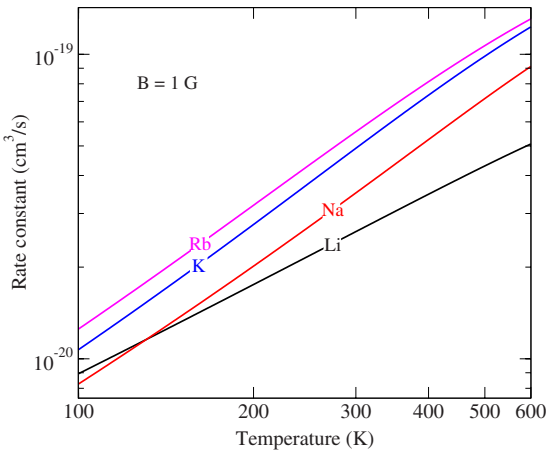

FIG. 8. (Color online) Rate constants for collision-induced spin exchange of Li, Na, K, and Rb in a gas of He as functions of temperature at a magnetic field of 1 G.

TABLE II. Calculated and measured rate constants for spin-exchange transitions in collisions of Li, Na, K, and Rb atoms with He. The rate constants are given in units of cm^3/s. References to experimental work are given where available. The "Theor." column contains the results of quantum scattering calculations described in the present work.

Atom	Temperature (K)	Γ_{SE} (Expt.)	Γ_{SE} (Theor.)	Reference
Li	400.0		3.5×10^{-20}	
	500.0		4.3×10^{-20}	
Na	583.15	$(6.1\pm0.6)\times10^{-20}$	8.8×10^{-20}	[14]
K	463.15	$(6.1\pm0.4)\times10^{-20}$	8.9×10^{-20}	[12,13]
	470.15	$(4.0\pm0.3)\times10^{-20}$	8.9×10^{-20}	[10]
Rb	360.0[a]	$(6.7\pm0.6)\times10^{-20}$	7.1×10^{-20}	[9]
	444.15	$(6.5\pm0.4)\times10^{-20}$	9.3×10^{-20}	[10]
	453.0	$(6.1\pm0.2)\times10^{-20}$	9.5×10^{-20}	[11]

[a]The lowest temperature of the measurement.

tion. Figure 3 shows that the *ab initio* Fermi contact interaction constant for Li-He increases less steeply with decreasing R than predicted by Eq. (21). Therefore, the spin-exchange rates calculated using the atomic model should have a stronger temperature dependence. The results shown in Figs. 7 and 8 confirm this supposition. The temperature dependence of the spin-exchange rate for Li-He clearly stands out, varying more slowly than for other alkali-metal atoms. Table II compares the experimental and calculated rate constants for spin-exchange collisions of Na, K, and Rb atoms with He at selected temperatures. Although the overall agreement with experiment is good, the theoretical rate constants are larger than the measured values by 30–50 %. Table II shows that the experimental spin-exchange rates are similar for different alkali-metal atoms and display no temperature dependence. In contrast, the calculated rate constants do have a weak temperature dependence, increasing by 20–30 % as the temperature varies from 360 to 550 K. Since our scattering calculations are exact, the origin of the discrepancy must be attributed to atomic model (21), which is probably not accurate enough to reproduce fine details of the R-dependent Fermi contact interaction.

The difference between the spin-relaxation rates for light (Li and Na) and heavy (K and Rb) alkali-metal atoms is not as large as one would expect from the analysis of Fig. 4, which shows that the hyperfine coupling for the heavier atoms is ~10 times stronger. The reason is that the inner turning points of the interaction potentials for K-He and Rb-He (marked by arrows in Fig. 4) are shifted to larger R, preventing the collision partners from reaching the region of strong Fermi contact interaction. In order to verify this hypothesis, we calculated the cross sections for K-He using the Li-He interaction potential, which is equivalent to shifting the K-He interaction potential to smaller R by $\sim 2a_0$. We found that this modification leads to an enhancement of the spin-exchange cross section by a factor of ~100. Such a dramatic effect reflects the exponential increase of the Fermi contact hyperfine interaction at small R shown in Fig. 4.

In Fig. 9, we plot the magnetic field dependence of the spin-exchange cross section for Rb-He at a collision energy

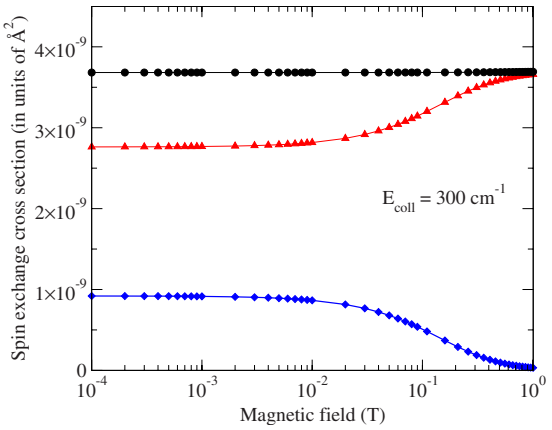

FIG. 9. (Color online) Magnetic field dependence of the cross sections for spin-exchange transitions $|F=2,m_F=2\rangle \rightarrow |F'=1,m_F'=1\rangle$ (triangles) and $|F=2,m_F=2\rangle \rightarrow |F'=2,m_F'=1\rangle$ (diamonds) in Rb-He collisions at a collision energy of 300 cm^{-1}. The total spin-exchange cross section is also shown (circles).

of 300 cm^{-1}. Although it appears that the total spin-exchange cross section is not sensitive to magnetic fields below 1 T, the probabilities for individual hyperfine transitions (shown by the arrows in Fig. 6) are altered to a significant extent. In particular, the F-conserving transition $|F=2,m_F=2\rangle \rightarrow |F'=2,m_F'=1\rangle$ is completely suppressed by magnetic fields on the order of 0.5 T. We find that the magnetic field suppression of the partial cross section occurs over a wide range of collision energies, from 1 to 300 cm^{-1}, and it seems to be insensitive to the collision energy.

E. Collisions at low temperatures

Collisional depolarization of the alkali-metal atoms in cryogenic He gas is of special interest for applications in magnetic trapping and evaporative cooling [3], atomic magnetometry [15], and quantum coherent optics [2]. Thus it would be interesting to investigate the dynamics of spin-exchange collisions in this heretofore unexplored regime. Figure 10 shows the spin-exchange cross sections as functions of collision energy at a magnetic field of 1 G. In the limit of zero collision energy, the cross sections vary as $E_c^{-1/2}$, in accordance with the Wigner threshold law for s-wave scattering [50]. The cross sections for Na, K, and Rb atoms follow the threshold behavior at $E_c < 0.01$ cm^{-1}. In the case of Li-He, the cross sections are notably larger and assume the $E_c^{-1/2}$ dependence only for collision energies below 10^{-4} cm^{-1}. This is because the long-range part of the Fermi contact interaction for Li-He decreases less slowly than for other alkali-metal atoms (see Fig. 4). The results shown in Figs. 4 and 10 thus illustrate that small variations in the Fermi contact interaction may lead to drastic changes in spin-exchange cross sections at ultralow collision energies.

Table III shows the rate constants for spin exchange in M-He collisions at a temperature of 0.5 K and magnetic field of 2 T. The spin-exchange rate for Li-He is the largest, as expected from the analysis of Fig. 10. It has been demonstrated [22] that spin exchange is the dominant inelastic loss

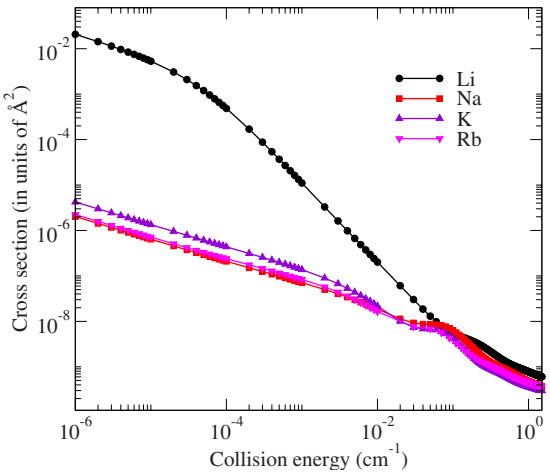

FIG. 10. (Color online) Cross sections for spin exchange in collisions of the alkali-metal atoms with He as functions of collision energy at a magnetic field of 1 G.

channel for light alkali-metal atoms (Li-K) at temperatures below 1 K. The calculated ratios of the rate constants for diffusion and inelastic scattering ($\sim 10^{11}$) are consistent with the upper bounds derived from magnetic trapping experiments with Li and K atoms [22]. Typical values of the elastic-to-inelastic ratios are 10^4 for transition-metal atoms [51], 10^4-10^5 for rare-earth atoms [52], 10^6 for CaH($^2\Sigma$) [4], and 10^5 for NH($^3\Sigma$) [53,54]. Table III illustrates that different alkali-metal atoms have similar spin-depolarization rates. We note that because of its long-range character, the anisotropic part of the hyperfine interaction (not considered in the present work) may affect the dynamics of spin-exchange collisions at low temperatures. As such, the results presented in Table III should be treated with caution. A rigorous study of the effects of anisotropic hyperfine interactions on spin-exchange collisions at low temperatures will be presented in a future publication.

IV. SUMMARY

We have presented a rigorous theoretical analysis of spin-exchange transitions in collisions of the alkali-metal atoms with He based on state-of-the-art *ab initio* calculations of the interaction potentials, Fermi contact interaction constants, and hyperfine pressure shifts. We have calculated the cross sections and rate constants for spin-exchange transitions in collisions of Li, Na, K, and Rb atoms with He over a wide range of temperatures. We have found good agreement between the calculated rate constants and the values measured in recent SEOP experiments with Na, K, and Rb atoms in a buffer gas of He.

TABLE III. Rate constants for diffusion (Γ_D) and spin exchange (Γ_{SE}) for Li, Na, K, and Rb atoms in a gas of ^{3}He at a temperature of 0.5 K. The rate constants are given in units of cm^3/s. Also shown are the calculated and measured upper bounds to the ratios Γ_D/Γ_{SE}. The calculated values are for $B=2$ T. The experimental estimates are taken from Ref. [22].

Atom	Γ_{SE}	Γ_D	Γ_D/Γ_{SE} (Theor.)	Γ_D/Γ_{SE} (Expt.)
Li	1.2×10^{-21}	1.5×10^{-10}	1.3×10^{11}	$>5.4\times10^5$
Na	6.4×10^{-22}	1.9×10^{-10}	3.0×10^{11}	
K	4.7×10^{-22}	1.8×10^{-10}	3.7×10^{11}	$>1.1\times10^8$
Rb	5.5×10^{-22}	1.8×10^{-10}	3.2×10^{11}	

Accurate *ab initio* calculations show that the variation with R of the Fermi contact interaction constant for Li-He is slower than that predicted by the atomic model. As a consequence, quantum scattering calculations based on the atomic model yield a positive temperature dependence of the rate constants for spin exchange in collisions of alkali-metal atoms with He. However, no temperature dependence was detected in previous SEOP experiments [9–14]. This disagreement suggests the need to go beyond the atomic model. An extension of the *ab initio* calculations presented in this work to heavier alkali-metal atoms would enable direct comparison with experimental data and may elucidate the role of anisotropic hyperfine interactions in spin-exchange dynamics [47].

The interaction potentials of the alkali-metal atoms with He are extremely shallow and their depths decrease from Li to Rb. For example, the *ab initio* interaction potential for Rb-He computed in this work has the well depth of 1.0 cm^{-1}, which is $\sim$7.5 times smaller than that of the He-He interaction [38]. These highly repulsive interactions prevent the formation of shape resonances in collisions of the Li, Na, K, and Rb atoms with ^{3}He. The hyperfine pressure shifts for Li-He calculated with the model of Oreto *et al.* [23] are in fairly good agreement with the present *ab initio* calculations. The remaining discrepancy can be attributed to the perturbation theory and Fermi contact approximation used to describe the mixing between the ground and electronically excited states of the alkali-metal atom induced by the interaction with He.

The *ab initio* approach presented in this work can be easily generalized to describe the dynamics of collisional spin exchange in non-S-state atoms and open-shell molecules. Measurements of spin-exchange transitions in collisions of atoms (such as Cr and N [55,56]) and molecules (such as O_2 [57]) with ^{3}He are valuable sources of information about the electronic structure and hyperfine interactions in these systems. Such measurements, accompanied by rigorous theoretical calculations, will help improve the efficiency of SEOP experiments by selecting the species with the optimal ratio of the rate constants for spin exchange and spin relaxation. A proper theoretical description of collision-induced spin relaxation is a key to accomplish this goal. We have demonstrated by a model calculation that the rate constant for spin relaxation in K-He collisions is a rapidly varying function of temperature [22]. The mechanism of the spin relaxation is determined by the term $\gamma(R)\hat{\ell}\cdot\hat{S}$ in the spin-dependent Hamiltonian (4). The spin-rotation constant $\gamma(R)$ can be expressed via the matrix elements of the spin-orbit interaction and nonadiabatic coupling between the ground ($^2\Sigma$) and the first excited ($^2\Pi$) electronic states of the M-He complex [58].

The results presented in Table III demonstrate that collisional spin depolarization of the alkali-metal atoms in cryo-

genic ^{3}He gas is 4–5 orders of magnitude slower than in other open-shell species such as the noble-metal atoms [16], transition-metal atoms [51], and NH molecules [53,54]. Such extraordinarily low inelastic rates may enable novel applications of buffer-gas-cooled alkali-metal atoms in precision spectroscopy, quantum optics, and quantum information processing [22]. In particular, using cold He gas to slow the diffusion of atoms to the cell walls may greatly increase the sensitivity of spectroscopic experiments to measure the electric dipole moment of the electron [59]. At large buffer-gas densities, the relaxation mechanisms due to atom-atom collisions are suppressed, which increases the maximum attainable atom density and may be used to enhance the sensitivity of atomic clocks and high-precision atomic magnetometers based on alkali-metal vapor cells [1,15].

ACKNOWLEDGMENTS

This work was supported by the Chemical Science, Geoscience, and Bioscience Division of the Office of Basic Energy Science, Office of Science, U.S. Department of Energy and NSF grants to the Harvard-MIT Center for Ultracold Atoms and the Institute for Theoretical Atomic, Molecular, and Optical Physics at Harvard University and Smithsonian Astrophysical Observatory.

APPENDIX: MATRIX ELEMENTS IN THE COUPLED BASIS

The matrix elements of the hyperfine interaction in coupled basis (13) are given by

$$\langle Fm_F|A\hat{I}\cdot\hat{S}|F'm_F'\rangle = \tfrac{1}{2}A[F(F+1)-I(I+1) - S(S+1)]\delta_{FF'}\delta_{m_F m_F'}. \quad \text{(A1)}$$

Note that the matrix elements do not depend on ℓ, m_ℓ, and $M_{I_{\mathrm{He}}}$. Similarly, the electrostatic interaction potential has only diagonal matrix elements

$$\langle Fm_F|V(R)|F'm_F'\rangle = \delta_{FF'}\delta_{m_F m_F'}V(R). \quad \text{(A2)}$$

The interaction with magnetic fields couples different hyperfine levels. Explicit expressions for the matrix elements can be obtained using the Wigner-Eckart theorem [60]. They are

$$\langle Fm_F|2\mu_0 B\hat{S}_z|F'm_F'\rangle = 2\mu_0 B(-)^{I+S+2F-m_F+1}[(2F+1)(2F'+1)]^{1/2} \times[(2S+1)S(S+1)]^{1/2}\begin{pmatrix} F & 1 & F' \\ -m_F & 0 & m_F' \end{pmatrix}\begin{Bmatrix} S & F & I \\ F' & S & 1 \end{Bmatrix}, \quad \text{(A3)}$$

where the symbols in parentheses and curly brackets are 3-j and 6-j symbols. The Fermi contact interaction can be written in tensor form as follows:

$$A_{\mathrm{F}}(R)\hat{I}_{\mathrm{He}}\cdot\hat{S} = A_{\mathrm{F}}(R)\sum_q (-)^q \hat{I}^{(1)}_{\mathrm{He},q}\cdot\hat{S}^{(1)}_q, \quad \text{(A4)}$$

where the subscripts q indicate the tensor components. The matrix elements can therefore be factorized as follows:

$$\langle I_{\mathrm{He}}M_{I_{\mathrm{He}}}|\langle Fm_F|A_{\mathrm{F}}(R)\hat{I}_{\mathrm{He}}\cdot\hat{S}|I_{\mathrm{He}}M'_{I_{\mathrm{He}}}\rangle|F'm'_F\rangle = A_{\mathrm{F}}(R)\sum_q (-)^q\langle I_{\mathrm{He}}M_{I_{\mathrm{He}}}|\hat{I}^{(1)}_{\mathrm{He},q}|I_{\mathrm{He}}M'_{I_{\mathrm{He}}}\rangle \times\langle Fm_F|\hat{S}^{(1)}_q|F'm'_F\rangle. \quad \text{(A5)}$$

Using the Wigner-Eckart theorem to evaluate each of the matrix elements on the right-hand side and collecting all the terms, we find

$$\langle I_{\mathrm{He}}M_{I_{\mathrm{He}}}|\langle Fm_F|A_{\mathrm{F}}(R)\hat{I}_{\mathrm{He}}\cdot\hat{S}|I_{\mathrm{He}}M'_{I_{\mathrm{He}}}\rangle|F'm'_F\rangle = (-)^{I_{\mathrm{He}}+2F+I+S+1-m_F-M_{I_{\mathrm{He}}}}[(2S+1)S(S+1)]^{1/2} \times[(2F+1)(2F'+1)]^{1/2}A_{\mathrm{F}}(R) \times\sum_q (-)^q\begin{pmatrix} I_{\mathrm{He}} & 1 & I'_{\mathrm{He}} \\ -M_{I_{\mathrm{He}}} & q & M'_{I_{\mathrm{He}}} \end{pmatrix} \times\begin{pmatrix} F & 1 & F' \\ -m_F & -q & m_F' \end{pmatrix}\begin{Bmatrix} S & F & I \\ F' & S & 1 \end{Bmatrix}. \quad \text{(A6)}$$

In order to test our numerical results, we performed scattering calculations using CC expansion (5) in terms of coupled basis functions (13). The resulting cross sections were fully identical to those obtained with the uncoupled basis of Sec. II.

[1] I. K. Kominis, T. W. Kornack, J. C. Allred, and M. V. Romalis, Nature (London) **422**, 596 (2003); I. K. Kominis, Phys. Lett. A **372**, 4877 (2008).

[2] T. Hong, A. V. Gorshkov, D. Patterson, A. S. Zibrov, J. M. Doyle, M. D. Lukin, and M. G. Prentiss, Phys. Rev. A **79**, 013806 (2009).

[3] J. M. Doyle, B. Friedrich, J. Kim, and D. Patterson, Phys. Rev. A **52**, R2515 (1995).

[4] J. D. Weinstein, R. deCarvalho, T. Guillet, B. Friedrich, and J. M. Doyle, Nature (London) **395**, 148 (1998).

[5] T. G. Walker and W. Happer, Rev. Mod. Phys. **69**, 629 (1997).

[6] T. G. Walker, J. H. Thywissen, and W. Happer, Phys. Rev. A **56**, 2090 (1997).

[7] P. L. Anthony *et al.*, Phys. Rev. Lett. **71**, 959 (1993).

[8] M. S. Albert, G. D. Cates, B. Driehuys, W. Happer, B. Saam, C. S. Springer, and A. Wishnia, Nature (London) **370**, 199 (1994).

[9] A. Ben-Amar Baranga, S. Appelt, M. V. Romalis, C. J. Erickson, A. R. Young, G. D. Cates, and W. Happer, Phys. Rev. Lett. **80**, 2801 (1998).

[10] G. Wang, Ph.D. thesis, California Institute of Technology, 2008 (unpublished).

[11] B. Larson, O. Häusser, P. P. J. Delheij, D. M. Whittal, and D. Thiessen, Phys. Rev. A **44**, 3108 (1991).
[12] E. Babcock, I. Nelson, S. Kadlecek, B. Driehuys, L. W. Anderson, F. W. Hersman, and T. G. Walker, Phys. Rev. Lett. **91**, 123003 (2003).
[13] W. C. Chen, T. R. Gentile, T. G. Walker, and E. Babcock, Phys. Rev. A **75**, 013416 (2007).
[14] P. I. Borel, L. V. Søgaard, W. E. Svendsen, and N. Andersen, Phys. Rev. A **67**, 062705 (2003).
[15] A. O. Sushkov and D. Budker, Phys. Rev. A **77**, 042707 (2008).
[16] N. Brahms, B. Newman, C. Johnson, T. Greytak, D. Kleppner, and J. M. Doyle, Phys. Rev. Lett. **101**, 103002 (2008).
[17] R. M. Herman, Phys. Rev. **136**, A1576 (1964).
[18] In this work, we consider collisions with the ^{3}He isotope.
[19] T. G. Walker, Phys. Rev. A **40**, 4959 (1989).
[20] E. Babcock, I. A. Nelson, S. Kadlecek, and T. G. Walker, Phys. Rev. A **71**, 013414 (2005).
[21] M. V. Romalis and G. D. Cates, Phys. Rev. A **58**, 3004 (1998).
[22] T. V. Tscherbul, P. Zhang, H. R. Sadeghpour, A. Dalgarno, N. Brahms, Y. S. Au, and J. M. Doyle, Phys. Rev. A **78**, 060703(R) (2008).
[23] P. J. Oreto, Y.-Y. Jau, A. B. Post, N. N. Kuzma, and W. Happer, Phys. Rev. A **69**, 042716 (2004).
[24] R. R. Freeman, E. M. Mattison, D. E. Pritchard, and D. Kleppner, J. Chem. Phys. **64**, 1194 (1976).
[25] D. E. Manolopoulos, J. Chem. Phys. **85**, 6425 (1986).
[26] P. Dehmer and L. Wharton, J. Chem. Phys. **57**, 4821 (1972).
[27] H. Partridge, J. R. Stallcop, and E. Levin, J. Chem. Phys. **115**, 6471 (2001).
[28] W. H. Press, S. A. Teukolsky, W. T. Vetterling, and B. P. Flannery, *Numerical Recipes in C* (Cambridge University Press, Cambridge, England, 1988), Chap. 15.5.
[29] C. Zhu, A. Dalgarno, S. G. Porsev, and A. Derevianko, Phys. Rev. A **70**, 032722 (2004).
[30] P. J. Knowles, C. Hampel, and H.-J. Werner, J. Chem. Phys. **99**, 5219 (1993).
[31] J. D. Watts, J. Gauss, and R. J. Bartlett, J. Chem. Phys. **98**, 8718 (1993).
[32] M. Douglas and N. M. Kroll, Ann. Phys. (N.Y.) **82**, 89 (1974).
[33] A. Wolf, M. Reiher, and B. A. Hess, J. Chem. Phys. **117**, 9215 (2002).
[34] B. O. Roos, V. Veryazov, and P.-O. Widmark, Theor. Chem. Acc. **111**, 345 (2004).
[35] EMSL basis set exchange, https://bse.pnl.gov/bse/portal
[36] S. F. Boys and F. Bernardi, Mol. Phys. **19**, 553 (1970).
[37] H.-J. Werner, P. J. Knowles, R. Lindh, F. R. Manby, M. Schütz, P. Celani, T. Korona, A. Mitrushenkov, G. Rauhut, T. B. Adler, R. D. Amos, A. Bernhardsson, A. Berning, D. L. Cooper, M. J. O. Deegan, A. J. Dobbyn, F. Eckert, E. Goll, C. Hampel, G. Hetzer, T. Hrenar, G. Knizia, C. Köppl, Y. Liu, A. W. Lloyd, R. A. Mata, A. J. May, S. J. McNicholas, W. Meyer, M. E. Mura, A. Nicklass, P. Palmieri, K. Pflüger, R. Pitzer, M. Reiher, U. Schumann, H. Stoll, A. J. Stone, R. Tarroni, T. Thorsteinsson, M. Wang, and A. Wolf, MOLPRO, a package of *ab initio* programs.
[38] M. Jeziorska, W. Cencek, K. Patkowski, B. Jeziorski, and K. Szalewicz, J. Chem. Phys. **127**, 124303 (2007).
[39] H. Konishi and K. Morokuma, Chem. Phys. Lett. **12**, 408 (1971).
[40] S. A. Perera, L. M. Salemi, and R. J. Bartlett, J. Chem. Phys. **106**, 4061 (1997).
[41] S. A. Perera, J. D. Watts, and R. J. Bartlett, J. Chem. Phys. **100**, 1425 (1994).
[42] H. Sekino and R. J. Bartlett, J. Chem. Phys. **82**, 4225 (1985).
[43] J. F. Stanton, J. Gauss, J. D. Watts, P. G. Szalay, R. J. Bartlett *et al.*, ACES II, Mainz-Austin-Budapest version, www.aces2.de
[44] D. E. Woon and T. H. Dunning, Jr., J. Chem. Phys. **100**, 2975 (1994).
[45] T. H. Dunning, Jr., J. Chem. Phys. **90**, 1007 (1989).
[46] Z.-C. Yan, D. K. McKenzie, and G. W. F. Drake, Phys. Rev. A **54**, 1322 (1996).
[47] D. K. Walter, W. Happer, and T. G. Walker, Phys. Rev. A **58**, 3642 (1998).
[48] H. P. Saha, Phys. Rev. A **48**, 1163 (1993).
[49] M. Marinescu, H. R. Sadeghpour, and A. Dalgarno, Phys. Rev. A **49**, 982 (1994).
[50] E. P. Wigner, Phys. Rev. **73**, 1002 (1948).
[51] R. V. Krems, J. Kłos, M. F. Rode, M. M. Szczęśniak, G. Chalasiński, and A. Dalgarno, Phys. Rev. Lett. **94**, 013202 (2005).
[52] C. I. Hancox, S. C. Doret, M. T. Hummon, L. Luo, and J. M. Doyle, Nature (London) **431**, 281 (2004).
[53] W. C. Campbell, E. Tsikata, Hsin-I. Lu, L. D. van Buuren, and J. M. Doyle, Phys. Rev. Lett. **98**, 213001 (2007).
[54] W. C. Campbell, T. V. Tscherbul, Hsin-I. Lu, E. Tsikata, R. V. Krems, and J. M. Doyle, Phys. Rev. Lett. **102**, 013003 (2009).
[55] J. D. Weinstein, R. deCarvalho, J. Kim, D. Patterson, B. Friedrich, and J. M. Doyle, Phys. Rev. A **57**, R3173 (1998).
[56] M. T. Hummon, W. C. Campbell, Hsin-I. Lu, E. Tsikata, Y. Wang, and J. M. Doyle, Phys. Rev. A **78**, 050702(R) (2008).
[57] B. Saam, W. Happer, and H. Middleton, Phys. Rev. A **52**, 862 (1995).
[58] V. V. Meshkov, E. A. Pazyuk, A. Zaitsevskii, A. V. Stolyarov, R. Brühl, and D. Zimmermann, J. Chem. Phys. **123**, 204307 (2005).
[59] M. Bijlsma, B. J. Verhaar, and D. J. Heinzen, Phys. Rev. A **49**, R4285 (1994).
[60] R. N. Zare, *Angular Momentum* (Wiley, New York, 1988).